IEEE Access
Multidisciplinary | Rapid Review | Open Access Journal

Received December 31, 2019, accepted January 18, 2020, date of publication January 24, 2020, date of current version February 14, 2020.

Digital Object Identifier 10.1109/ACCESS.2020.2969387

MIMO Adaptive Bspline-Based Wavelet NeuroFuzzy Control for Multi-Type FACTS

RABIAH BADAR[1], MOHAMMAD ZUBAIR KHAN[2], AND MUHAMMAD AWAIS JAVED[1], (Senior Member, IEEE)

[1]Electrical and Computer Engineering Department, COMSATS University Islamabad, Islamabad 45550, Pakistan
[2]Department of Computer Science, College of Computer Science and Engineering, Taibah University, Madinah 41477, Saudi Arabia

Corresponding authors: Rabiah Badar (rabiah.badar@comsats.edu.pk) and Mohammad Zubair Khan (mkhanb@taibahu.edu.sa)

ABSTRACT Motivated by the synergistic integration of soft computing paradigms this paper introduces a fully adaptive multiple-input-multiple-output NeuroFuzzy control for multi-type Flexible AC Transmission Systems (FACTS) to damp low frequency oscillations. The novel control strategy integrates the complementary features of locally controllable fuzzy Bspline membership functions and robust wavelet neural networks in NeuroFuzzy structure. The gradient decent based back-propagation mechanism used for parameters update has been optimized using online Adaptive Learning Rates (ALRs). The stability of the proposed algorithm has been ensured by deriving an upper bound on ALRs using Lyapunov stability criteria. The application of this controller to provide damping signals to various FACTS controllers like Static Synchronous Series Compensator (SSSC) and Static Synchronous Compensator (STATCOM) can effectively enhance the dynamic stability of the system. A benchmark multi-machine power system has been used for performance validation of the controller by applying various faults under different loading scenarios. Conventional Lead-Lag and NeuroFuzzy controls have been considered for comparative evaluation using nonlinear time and frequency domain techniques to reveal that the proposed control performs better in different operating regions. Furthermore, the graphical results obtained from time and frequency domain simulations have been quantified numerically using different performance indices and Energy Spectral Density (ESD), respectively. The temporal, spectral and numerical analysis confirms the superior performance of the proposed control scheme.

INDEX TERMS Bspline, FACTS, MIMO adaptive control, multi-machine power system, NeuroFuzzy, wavelets.

I. INTRODUCTION

Electric power systems and their controls can be regarded as collection of many subsystems which makes them highly complex, nonlinear and multivariable dynamical systems. One of the most challenging tasks for widespread geographical structure of power systems, spanning over countries or even continents, is huge power transmission to the entire network. Bulk power transmission causes overloading of certain transmission lines, thus deteriorating the power quality and overall stability. The underlying controls, installed in early days of power system installations, were too simple to cope with rapidly changing dynamics of the system. Therefore, power systems were operated with large stability margins with respect to their thermal limits to ensure the stability, however, this resulted in deployment of additional infrastructure. On contrary, the environmental, economic and geographic constraints have restricted the physical growth of existing power systems. Moreover, the security and permanency of the whole system has further been jeopardized due to deregulation of electricity market forcing the reduction in operating margins of physical limits of transmission system. Another important factor consistently threatening the stability is Low Frequency Oscillations (LFOs) anticipated from discrete fault events like symmetrical or unsymmetrical faults and equipment failures etc.

This background has introduced the effective utilization of installed power network without further expansion of existing transmission system as one of the challenging research dimensions. LFOs may range from 0.2 to 2 Hz and can be

The associate editor coordinating the review of this manuscript and approving it for publication was Canbing Li.

characterized as Local or Interarea Modes of Oscillations (LIMOs) based on the number of affected areas and generating units. A single generator oscillating with respect to the rest of the network or a group of generators oscillating in the same area of a large network cause Local Mode of Oscillations (LMOs) with typical frequency spectrum of 0.8 to 2 Hz. The frequency of Interarea Mode of Oscillations (IMOs) ranges from 0.2 to 0.8 Hz involving a group of generators in one area oscillating against the generating units of another area.

In pursuant of efficient curative actions, researchers found that line power flow is governed by three factors; the sending and receiving end voltage magnitudes, angle between them or impedance of the line. The control of one or more of these parameters can control the active as well as reactive power flow. This caused the advent of Flexible AC Transmission Systems (FACTS) which can control the line power flow to improve the voltage profile. However, the additional goal of damping LFOs is achieved by exploiting an auxiliary damping control (ADC) for FACTS [1].

In literature, many Multiple Input Single Output (MISO) and MIMO controls using conventional and NeuroFuzy techniques have been presented for FACTS [2]–[8]. However, they use either single FACTS device or multiple FACTS controllers of same type which limits their application to single machine or small-scale power systems. In [9], intelligent coordinated control for wide area FACTS installation has been proposed considering only the shunt FACTS controllers. An evolutionary control technique to tune the parameters of conventional LFOs damping control has been proposed in [10]. The control design involves system linearization and thus validated only for small signal stability. In addition to this, most of the existing NeuroFuzzy controls are either linear in nature or not fully adaptive, involving computationally complex parameters initialization and tuning techniques. Furthermore, they use globally tuned membership functions which affects the robustness of the controller for nonlinear dynamic systems [11].

In this research, MIMO Bspline based wavelet NeuroFuzzy control has been proposed with Adaptive Learning Rates (ALRs) for power system installed with multi-type FACTS. The utilization of multi-type FACTS not only provides better control for large power systems but also helps to improve the dynamic performance of overall system. The proposed control utilizes Gaussian Bspline membership functions with adaptive characteristics. Bspline membership functions are locally controllable functions which can efficiently translate the modelling uncertainties to the rule base of fuzzy inference system. Furthermore, they help to improve the smoothness of the control effort which in turn minimizes the switching losses in power electronics based devices like FACTS. The parameters of the proposed control scheme are tuned online based on the current estimate of the plant model. MIMO identifier block is used to provide system Jacobean to control block. No offline training of either control or identifier is required.

As per author's prime survey the novel contribution of this research is

- the presentation of a systematic procedure for designing a multivariable supplementary damping control for FACTS using Bspline based wavelet Neural Network (NN).
- the performance validation and comparative evaluation of proposed Hybrid Bspline Wavelet Control (HBsWC), Adaptive NeuroFuzzy TSK Control (ANFTSC) and the conventional Lead-Lag Control (LLC) against different disturbances and operating conditions.
- the damping performance investigation using frequency domain analysis.
- the stability analysis of ALRs based MIMO control.

The primary goal of this article is not to focus the operational and modeling details of the system as it has already widely been discussed in literature. The detailed system modeling can be found in our earlier work [12].

The rest of the paper is arranged as follows; section II presents the control system design and formulation. The control algorithm and adaptation mechanism are given in section III. Section IV deals with the stability analysis of identifier and controller. Section V presents the detailed discussion of the simulation results. Section VI concludes the findings of this research with description of some interesting future dimensions of this work.

II. CONTROL SYSTEM DESIGN

The dynamic model of different power system components like generators, FACTS and their accompanying controls comprising many differential and algebraic equations can be combined in the following generalized form [13];

$$\begin{bmatrix} \boldsymbol{v} \\ \mathbf{0} \\ \boldsymbol{w} \end{bmatrix} = \begin{bmatrix} l(\boldsymbol{v}, z, \boldsymbol{u}) \\ m(\boldsymbol{v}, z, \boldsymbol{u}) \\ n(\boldsymbol{v}, z) \end{bmatrix} = \Phi(\boldsymbol{v}, \boldsymbol{w}, \boldsymbol{u}) \tag{1}$$

where, $\boldsymbol{v} \in \Re^p$, $\boldsymbol{w} \in \Re^m$, $z \in \Re^n$ and $\boldsymbol{u} \in \Re^q$ is the vector representation of dynamic sates of loads, generators and controllers, output variables, the steady-state algebraic parameters and inputs, respectively. The nonlinear function $l : \Re^p \times \Re^n \times \Re^q \to \Re^p$ represents the nonlinear differential equations, $m : \Re^p \times \Re^n \times \Re^q \to \Re^n$ defines algebraic constraints; $n : \Re^p \times \Re^n \to \Re^m$ describes the output variables and $\Phi : \Re^L \times \Re^q \to \Re^L$ is the nonlinear function with $L = p + n$. In the event of discrete faults, the system dynamics given in (1) may vary. Depending upon the nature of fault the post-fault system equilibrium can be restored either at pre-fault or some new equilibrium point.

The objective is to design a novel ADC to generate $\boldsymbol{u}$ such that $\boldsymbol{v}^* - \boldsymbol{v} \to \varepsilon$, where, $\boldsymbol{v}^*$ is the reference equilibrium state and $\varepsilon > 0$ is very small value, to ensure that the closed-loop system is globally stable.

Fig. 1 describes the complete system structure with its control and adaptation mechanisms. The structure comprises three main blocks i.e., a plant '$\mathbb{P}$' comprising power system installed with FACTS, Hybrid NeuroFuzzy Bspline based

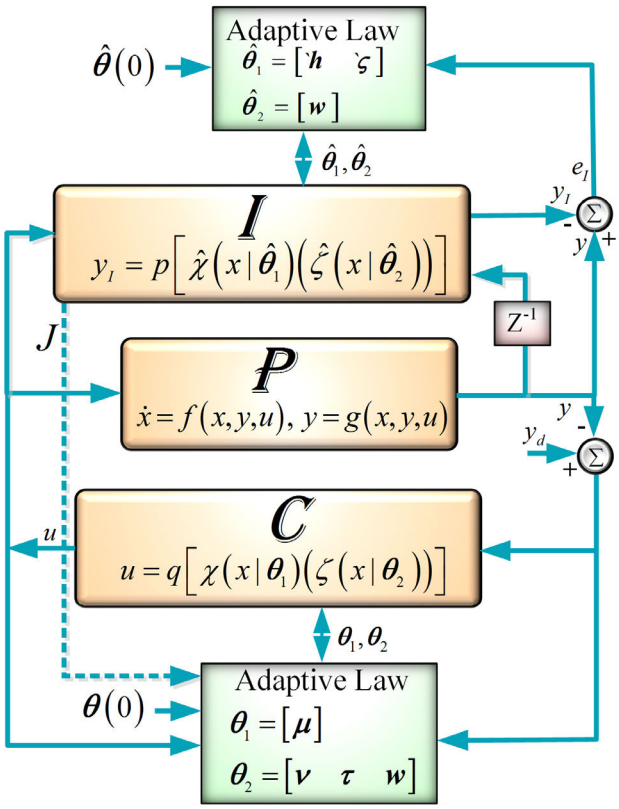

FIGURE 1. Closed-loop structure of direct/indirect control strategies.

wavelet control '$\mathbb{C}$' and adaptive NeuroFuzzy TSK based identification block '$\mathbb{I}$'. The two adaptation blocks are used for online adaptation of identifier and control block parameters.

The identifier provides online model of the plant thus making the overall scheme as indirect adaptive control. However, the proposed control scheme can also be modified for direct adaptive control by approximating the Jacobean used in adaptation mechanism as identity matrix.

The adaptation of control block parameters is done using relative rotor speed and power deviations and their derivatives such that $\left[\boldsymbol{w}_d \ \boldsymbol{w}\right] = \left[\boldsymbol{y}_d \ \boldsymbol{y}\right] = \left[\Delta\omega_d \ \Delta P_d \ \Delta\omega \ \Delta P\right]$, where $\boldsymbol{y}_d$ and $\boldsymbol{y}$ are the desired and actual output vectors of plant, respectively. The voltage injected by FACTS is regulated based on PWM parameters based on the difference of control block output and measured injected voltage.

The online plant sensitivity measure is provided by Adaptive NeuroFuzzy TSK based identifier in the form of plant Jacobean. Identification block inputs are the control output and delayed plant output.

A. CONTROL PROBLEM FORMULATION

Consider a NeuroFuzzy control, formulated by an unknown MIMO nonlinear function q, of the form:

$$\boldsymbol{u} = q\left(\varpi, \boldsymbol{\theta}\right) \tag{2}$$

where, $\varpi = \left[\boldsymbol{e} \ \dot{\boldsymbol{e}}\right]$ is the error input vector such that $e_i = y_{d_i} - y_i$ and $\dot{e}_i\left(k\right) = e_i\left(k\right) - e_i\left(k-1\right)$. $\boldsymbol{u} = \left[u_1 \ u_2 \ \cdots \ u_k\right]$ is the controller output vector.

The control objective is to adapt the controller parameters such that the derived controller output is upper bounded and the deviation of output plant variables from nominal equilibrium point vanishes asymptotically. The present instant value of plant estimate, used to update controller parameters, is provided by identifier, given as:

$$\boldsymbol{y}_I = p\left(\hat{\varpi}, \hat{\boldsymbol{\theta}}\right) \tag{3}$$

where, p and $\boldsymbol{y}_I = \left[y_{I_1} \ y_{I_2} \ \cdots \ y_{I_k}\right]$ represent MIMO identifier function and identifier output vector, respectively. $\hat{\varpi}$ is vector of input vectors formed by the controller outputs and delayed outputs of plant.

In (2) and (3), $\hat{\boldsymbol{\theta}}_i, \boldsymbol{\theta}_i$ represent the adaptation parameters vectors for identification and control block, respectively, with index $i = 1$ for antecedent part and '2' for consequent part.

Assumption: The proposed NeuroFuzzy based identifier or controller follows the assumption that the network structure is predefined in terms of number of inputs, membership and consequent functions and rules as per designer's choice.

The detail of each NeuroFuzzy structure contained in identification or control block, shown in Fig. 2, is given in the following sections.

III. PROPOSED MIMO ONLINE HBSWC

The proposed hybrid architecture, shown in Fig. 2, is governed by NeuroFuzzy rules generalized as:

$$\begin{aligned}&\Im_j : IF\ x_1 is \mu_{1j} \quad AND\ x_2\ is\ \mu_{2j} \cdots AND\ x_m\ is\ \mu_{mj}\\ &THEN\ \psi_j^1 = \zeta_j^1 \quad AND\ \psi_j^2 = \zeta_j^2 \cdots AND\ \psi_j^k = \zeta_j^k\end{aligned}$$

where, $\Im_j$ is the *jth* fuzzy rule such that $x \in \{x_1, x_2, \cdots, x_m\} \in U \subset \Re^m$ and $\zeta_j \in V \subset \Re$ represent the crisp input and *jth* nonlinear consequent function.

NeuroFuzzy rules are structured in following layered fashion:

Layer 1: is responsible for input data acquisition from the environment for NeuroFuzzy architecture.

Layer 2: processes the input space and transforms the crisp data to fuzzy values using membership functions, given as:

$$\mu_{ij} = \chi\left(x_i, \boldsymbol{\theta}_1\right) \tag{4}$$

where, χ is the fuzzy membership function. $\boldsymbol{\theta}_1$ represents the adaptation parameters vector for antecedent part and becomes $\hat{\boldsymbol{\theta}}_1$ for identification block. i and j are the indices for input and membership function, respectively.

Layer 3: is used to calculate the rule firing strength:

$$\wp_j = \prod_{i=1}^{m} \mu_{ij} \tag{5}$$

Layer 4: starts to imply the consequent part such that each node processes the adaptive nonlinear function $\zeta_j^p\left(x, \boldsymbol{\theta}_2^p\right)$ of j th rule and p th output. Where, $\boldsymbol{\theta}_2$ is the consequent parameters adaptation vector.

Layer 5: produces the product term, using outputs of layers 3 and 4, to be processed by the following layer.

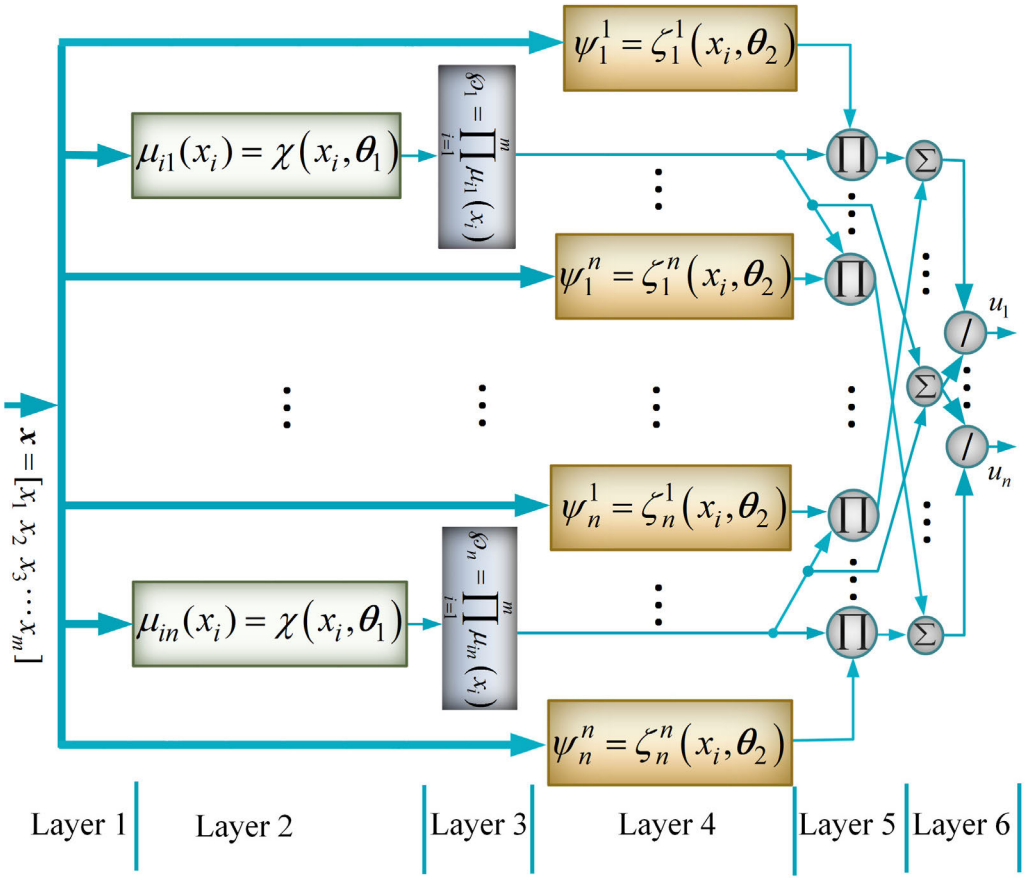

FIGURE 2. Generalized NeuroFuzzy network with adaptive parameters.

Layer 6: utilizes Center of Gravity (COG) method for defuzzification to finally calculate the network output, given as:

$$u_p = \frac{\sum_{j=1}^{n} \wp_j \zeta_j^p}{\sum_{j=1}^{n} \wp_j} \quad where, \; 1 \le p \le k \tag{6}$$

The identification block contains simple TSK NeuroFuzzy structure with input Gaussian membership functions and polynomial output functions to avoid the computational complexity of controller.

A. ADAPTATION ALGORITHM

The identification block contains simple TSK based NeuroFuzzy structure whose details and online parameters adaptation can be found in [12].

Online adaptation of control block parameters is carried out by minimizing the following cost function using gradient descent optimization with back-propagation algorithm:

$$J_C = \frac{1}{2}\left(\boldsymbol{e}^T\boldsymbol{e} + \boldsymbol{e}_v^T\boldsymbol{e}_v\right) \tag{7}$$

Here, $\boldsymbol{e} = \begin{bmatrix} e_1 & e_2 & \cdots & e_k \end{bmatrix}$ defines the error vector such that $e_i = y_{d_i} - y_i$ and $\boldsymbol{e}_v = \begin{bmatrix} e_{v_1} & e_{v_2} & \cdots & e_{v_k} \end{bmatrix}$, where $e_{v_i} = \sqrt{\hbar_i} u_i$.

The antecedent part of control block contains Bspline membership functions to fuzzify the linguistic variable, given as;

$$\mu_{ij}(x_i) = \sum_{i=0}^{n} v_i \xi_{i,\ell}(x_i) \tag{8}$$

Equation (8) describes the locally controllable Bspline membership function with 'n+1' control points. v_i denotes the control points and $\xi_{i,\ell}(x_i) = \xi(x|\tau_0, \tau_1, \cdots, \tau_{n+k})$ are the basis functions used to construct Bspline membership function. The following recursive formula is used to define these basis functions;

$$\xi_{i,\ell}(\tau) = \left(\frac{\tau - \tau_i}{\tau_{i+\ell-1} - \tau_i}\right)\xi_{i,\ell-1}(\tau) + \left(\frac{\tau_{i+\ell} - \tau}{\tau_{i+\ell} - \tau_{i+1}}\right)\xi_{i+1,\ell-1}(\tau), \; \tau_i \le \tau < \tau_{i+\ell} \tag{9}$$

$$\xi_{i,1}(\tau) = \begin{cases} 1, & \text{if } \tau_i \le \tau < \tau_{i+1} \\ 0 & \text{otherwise} \end{cases} \tag{10}$$

where, $T = \{\tau_0, \tau_1, \cdots \tau_n\}$ represents a monotonically increasing sequence of real numbers, called knot vector, used to construct Bspline curves. Bspline membership function of order 2 with fixed number of control points and knot vector is used in this work.

The consequent nodes contain Morlet wavelet functions NNs with *jth* wavelet output calculated as:

$$\psi_j = w_j \sum_{r=1}^{n} \phi_r \tag{11}$$

where,

$$\phi_r(x_i) = \cos(5\rho_r) e^{-\frac{\rho_r^2}{2}} \tag{12}$$

where, $\rho_r = \frac{x_i - \tau_r}{\upsilon_r}$. Here, τ_r represents the translation and υ_r denotes the dilation factor of the wavelet functions.

The generalized form of update law used in adaptation mechanism is given as:

$$\boldsymbol{\theta}_p(k+1) = \boldsymbol{\theta}_p(k) - \boldsymbol{\eta} \frac{\partial J_C}{\partial \boldsymbol{\theta}_p} \tag{13}$$

where, p and $\boldsymbol{\theta}$ represents the output index and the vector containing adaptation parameters, respectively. The Lyapunov stability criteria based ALRs are contained in $\boldsymbol{\eta}$.

The gradient of the cost function is calculated as;

$$\frac{\partial J_C}{\partial \boldsymbol{\theta}_p} = -\boldsymbol{e}\boldsymbol{J}\boldsymbol{U}' + \boldsymbol{e}_v \boldsymbol{J}_{\hbar} \boldsymbol{U}' \tag{14}$$

where, $\boldsymbol{U}' = \left[\frac{\partial u_1}{\partial \boldsymbol{\theta}_p} \ \frac{\partial u_2}{\partial \boldsymbol{\theta}_p} \ \cdots \ \frac{\partial u_k}{\partial \boldsymbol{\theta}_p} \right]^T$.

Also, $\boldsymbol{J}_{\hbar} = diag\left[\sqrt{\hbar_{ii}}\right]_{k\times k}$ and $\boldsymbol{J} = \left[\frac{\partial y_i}{\partial u_j}\right]_{k\times k}$ denotes the penalty matrices and system Jacobean, respectively, with $i = 1, 2, \cdots, k$ and $j = 1, 2, \cdots, k$.

Differentials in $\boldsymbol{U}'$ can be simplified by using chain rules of calculus.

Following relations can be obtained after simplification.

$$\frac{\partial u_p}{\partial \mu_{ij}^p} = \wp_j \left(\frac{\zeta_j^p - u_p}{\mu_{ij}^p \sum_j \wp_j} \right) \tag{15}$$

$$\frac{\partial u_p}{\partial \tau_{ij}^p} = \wp_j w_\ell^p \left(\frac{\cos\left(5\rho_{ij}^p\right) e^{-0.5\rho_{ij}^{(p)^2}} \rho_{ij}^p + 5\sin\left(5\rho_{ij}^p\right) e^{-0.5\rho_{ij}^{(p)^2}}}{\upsilon_{ij}^p \sum_j \wp_j} \right) \tag{16}$$

$$\frac{\partial u_p}{\partial \upsilon_{ij}^p} = \wp_j w_\ell^p \rho_{ij}^p \left(\frac{\cos\left(5\rho_{ij}^p\right) e^{-0.5q_{ij}^{(p)2}} \rho_{ij}^p + 5\sin\left(5\rho_{ij}^p\right) e^{-0.5\rho_{ij}^{(p)^2}}}{\upsilon_{ij}^p \sum_j \wp_j} \right) \tag{17}$$

$$\frac{\partial u_p}{\partial w_{ij}^p} = \frac{\wp_j \psi_{ij}^p}{\sum_j \wp_j} \tag{18}$$

The plant Jacobean term is calculated online using identification block as follows:

$$\frac{\partial y_p}{\partial u_k} = \sum_j \wp_j \left(\frac{-2\left(\zeta_j^p - y_{I_i}\right)}{\sum_j \wp_j} \cdot \frac{\left(u_k - h_{ij}\right)}{\varsigma_{ij}^2} + w_{ij}^p \right) \tag{19}$$

Here, $\wp_j$, 'ζ_j^p, 'h_{ij}, 'ς_{ij} are the identification block parameters.

Update laws for parameters of control block can be found using (15)-(18) in (13) and (14).

IV. STABILITY ANALYSIS OF THE PROPOSED CONTROL SCHEME

A. STABILITY ANALYSIS OF HBSWC

The convergence speed of gradient descent learning algorithm depends upon the optimal choice of learning rate. Lyapunov based ALRs can effectively be used to guarantee the convergence. Control block parameters adaptation has been done through backpropagation learning algorithm using gradient descent technique to minimize the following cost function:

$$J_C = \frac{1}{2}\left(\boldsymbol{e}^T\boldsymbol{e} + \boldsymbol{e}_v^T\boldsymbol{e}_v\right) \tag{20}$$

Here, the error vectors are defined as, $\boldsymbol{e} = \left[e_1 \ e_2 \ \cdots \ e_k \right]$ such that $e_i = y_{d_i} - y_i$ and $\boldsymbol{e}_v = \left[e_{v_1} \ e_{v_2} \ \cdots \ e_{v_k} \right]$ such that $e_{v_i} = \sqrt{\hbar_i} u_i$. The generalized parameters update law is given as;

$$\boldsymbol{\theta}_p(k+1) = \boldsymbol{\theta}_p(k) - \boldsymbol{\eta} \frac{\partial J_C}{\partial \boldsymbol{\theta}_p} \tag{21}$$

where, $\boldsymbol{\theta}_p$ is the adaptation parameters vector.

$\boldsymbol{\eta}$ is the ALRs vector based on Lyapunov stability criteria. The ALRs given in (13) are governed by the following theorem using Lyapunov stability criteria.

Theorem 1: Let η be the learning rate for pth output affected by the antecedent parameters vector $\boldsymbol{\theta}$ of NeuroFuzzy control. $\boldsymbol{\Lambda}_p$ and $\boldsymbol{\Lambda}_{\max}^p$ are defined as $\boldsymbol{\Lambda}_p = \frac{\partial u_p}{\partial \boldsymbol{\theta}}$ and $\boldsymbol{\Lambda}_{\max}^p = \max \left\| \boldsymbol{\Lambda}^p \right\|$, where, $\|.\|$ is the Euclidean norm in $\Re^p$.

Then the convergence is guaranteed if the learning rates are chosen as follows;

$$0 < \eta < \frac{2}{\left\{ \left(\frac{\partial y_1}{\partial u_c}\right)^2 + \left(\frac{\partial y_2}{\partial u_c}\right)^2 + \hbar_p \right\} \left\| \frac{\partial u_p}{\partial \boldsymbol{\theta}} \right\|_{\max}^2} \tag{22}$$

Where, $\frac{\partial y_i}{\partial u_p} = \left[\frac{\partial y_i}{\partial u_1} \ \frac{\partial y_i}{\partial u_2} \right]$, $\sqrt{\hbar_p} = \left[\sqrt{\hbar_1} \ \sqrt{\hbar_2} \right]$, $\frac{\partial u_p}{\partial \boldsymbol{\theta}} = \left[\frac{\partial u_1}{\partial \boldsymbol{\theta}} \ \frac{\partial u_2}{\partial \boldsymbol{\theta}} \right]^T$ *and* $i = 1, 2$

Proof: Consider the following discrete type Lyapunov function,

$$V_C(k) = \frac{1}{2} \sum_{i=1}^{2} \left(e_i^2(k) + e_{v_i}^2(k) \right) \tag{23}$$

Then, change in Lyapunov function is given as;

$$\Delta V_C(k) = V_C(k+1) - V_C(k) \tag{24}$$

and

$$e_i(k+1) = e_i(k) + \Delta e_i(k) \tag{25}$$

$$\Delta V_C(k) = \sum_{i=1}^{2} \left(\begin{matrix} \frac{\Delta e_i^2(k)}{2} + \Delta e_i(k)\, e_i(k) + \frac{\Delta e_{v_i}^2(k)}{2} \\ + \Delta e_{v_i}(k)\, e_{v_i}(k) \end{matrix} \right) \tag{26}$$

where, $\Delta e_i = \left[\frac{\partial e_i}{\partial \boldsymbol{\Omega}}\right]^T \Delta \boldsymbol{\Omega}$, $\Delta \boldsymbol{\theta} = -\eta \frac{\partial J_C}{\partial \boldsymbol{\theta}}$

$$J_C = \frac{1}{2}\sum_{i=1}^{2}\left(y_{d_i} - y_i\right)^2 + \frac{1}{2}\sum_{i=1}^{2}\hbar_i u_i^2 \tag{27}$$

$$\Rightarrow \frac{\partial J_C}{\partial \boldsymbol{\theta}} = A + B \tag{28}$$

where,

$$A = \left(-e_1\frac{\partial y_1}{\partial u_1} - e_2\frac{\partial y_2}{\partial u_1} + \sqrt{\hbar_1}e_{u_1}\right),$$

$$B = \left(-e_1\frac{\partial y_1}{\partial u_2} - e_2\frac{\partial y_2}{\partial u_2} + \sqrt{\hbar_2}e_{u_2}\right)$$

$$\Rightarrow \Delta e_1 = \eta\left[y'_{11}.u'_1 + y'_{12}.u'_2\right]^T\left(Au'_1 + Bu'_2\right) \tag{29}$$

where, $y'_{11} = \frac{\partial y_1}{\partial u_1}$, $y'_{12} = \frac{\partial y_1}{\partial u_2}$, $u'_1 = \frac{\partial u_1}{\partial \boldsymbol{\theta}}$, $u'_2 = \frac{\partial u_2}{\partial \boldsymbol{\theta}}$

$$\Delta e_1 = \eta\left\{\begin{matrix} y'_{11}\left\|u'_1\right\|^2 A + y'_{11}\left[u'_1\right]^T\left[u'_2\right]B \\ + y'_{12}\left\|u'_2\right\|^2 B + Ay'_{12}\left[u'_2\right]^T\left[u'_1\right] \end{matrix}\right\} \tag{30}$$

Similarly,

$$\Delta e_2 = \eta\left\{\begin{matrix} y'_{21}\left\|u'_1\right\|^2 A + y'_{22}\left[u'_2\right]^T\left[u'_1\right]A \\ + y'_{22}\left\|u'_2\right\|^2 B + By'_{21}\left[u'_1\right]^T\left[u'_2\right] \end{matrix}\right\} \tag{31}$$

where, $y'_{21} = \frac{\partial y_2}{\partial u_1}$, $y'_{22} = \frac{\partial y_2}{\partial u_2}$

$$\Delta e_{u_1} = -\eta\left[\sqrt{\hbar_1}\ u'_1\right]\frac{\partial J_C}{\partial \boldsymbol{\Omega}}$$

$$= -\eta\sqrt{\hbar_1}\left(\left\|u'_1\right\|^2 A + B\left[u'_1\right]^T\left[u'_2\right]\right) \tag{32}$$

$$\Delta e_{u_2} = -\eta\left[\sqrt{\hbar_2}\ u'_2\right]\frac{\partial J_C}{\partial \boldsymbol{\Omega}}$$

$$= -\eta\sqrt{\hbar_1}\left(\left\|u'_2\right\|^2 B + A\left[u'_2\right]^T\left[u'_1\right]\right) \tag{33}$$

Using $\left[u'_2\right]^T\left[u'_1\right] = \left[u'_1\right]^T\left[u'_2\right] = C$ and $\left\|u'_1\right\|^2\left\|u'_2\right\|^2 = C^2$

$$\Delta V_C(k) = \eta\left\{e_1\left(\begin{matrix} y'_{11}\left\|u'_1\right\|^2 A + y'_{11}BC \\ + y'_{12}\left\|u'_2\right\|^2 B + y'_{12}AC \end{matrix}\right) + e_2\left(y'_{21}\left\|u'_1\right\|^2 A + y'_{22}AC + y'_{22}\left\|u'_2\right\|^2 B + y'_{21}BC\right) - e_{u_1}\sqrt{\hbar_1}\left(\left\|u'_1\right\|^2 A + BC\right) - e_{u_2}\sqrt{\hbar_2}\left(AC + \left\|u'_2\right\|^2 B\right)\right\} + \frac{\eta^2}{2}\left\{\left(y'_{11}\left\|u'_1\right\|^2 A + y'_{11}BC + y'_{12}\left\|u'_2\right\|^2 B + y'_{12}AC\right)^2 + \left(y'_{21}\left\|u'_1\right\|^2 A + y'_{22}AC + y'_{22}\left\|u'_2\right\|^2 B + y'_{21}BC\right)^2\right\} + \hbar_1\left(A\left\|u'_1\right\|^2 + BC\right)^2 + \hbar_2\left(AC + B\left\|u'_2\right\|^2\right)^2 \tag{34}$$

$$\Delta V_C = \eta\left\{A\left\|u'_1\right\|^2\overbrace{\left(e_1y'_{11} + e_2y'_{21} - e_{u_1}\sqrt{\hbar_1}\right)}^{-A} + B\left\|u'_2\right\|^2\overbrace{\left(e_1y'_{12} + e_2y'_{22} - e_{u_2}\sqrt{\hbar_2}\right)}^{-B} + BC\overbrace{\left(e_1y'_{11} + e_2y'_{21} - e_{u_1}\sqrt{\hbar_1}\right)}^{-A} + AC\overbrace{\left(e_1y'_{12} + e_2y'_{22} - e_{u_2}\sqrt{\hbar_2}\right)}^{-B}\right\} + \frac{\eta^2}{2}\left\{A^2{y'_{11}}^2\left\|u'_1\right\|^4 + {y'_{11}}^2B^2C^2 + {y'_{12}}^2\left\|u'_2\right\|^4B^2 + {y'_{12}}^2A^2C^2 + 2ABC{y'_{11}}^2\left\|u'_1\right\|^2 + 2y'_{11}y'_{12}AB\left\|u'_1\right\|^2\left\|u'_2\right\|^2 + 2y'_{11}y'_{12}A^2C\left\|u'_1\right\|^2 + 2y'_{11}y'_{12}B^2C\left\|u'_2\right\|^2 + 2y'_{11}y'_{12}ABC^2 + {y'_{12}}^2ABC\left\|u'_2\right\|^2 + {y'_{21}}^2A^2\left\|u'_1\right\|^4 + A^2C^2{y'_{22}}^2 + B^2C^2{y'_{21}} + B^2{y'_{22}}^2\left\|u'_2\right\|^4 + 2y'_{21}y'_{22}A^2C\left\|u'_1\right\|^2 + 2{y'_{21}}^2ABC\left\|u'_1\right\|^2 + 2ABy'_{21}y'_{22}\left\|u'_1\right\|^2\left\|u'_2\right\|^2 + 2ABC^2y'_{21}y'_{22} + 2ABC{y'_{22}}^2\left\|u'_2\right\|^2 + 2B^2Cy'_{21}y'_{22}\left\|u'_2\right\|^2 + \hbar_1\left\|u'_1\right\|^4A^2 + \hbar_1B^2C^2 + 2ABC\hbar_1\left\|u'_1\right\|^2 + \hbar_2\left\|u'_2\right\|^2B^2 + A^2C^2\hbar_2 + 2ABC\hbar_2\left\|u'_2\right\|^2\right\} \tag{35}$$

$$= \eta\left\{-A^2\left\|u'_1\right\|^2 - B^2\left\|u'_2\right\|^2 - 2ABC\right\} + \frac{\eta^2}{2}\left[2ABC\left\{\left\|u'_1\right\|^2\left({y'_{11}}^2 + {y'_{21}}^2 + \hbar_1\right) + \left\|u'_2\right\|^2 \times \left({y'_{12}}^2 + {y'_{22}}^2 + \hbar_2\right) + \left[y'_{11}y'_{12} + y'_{21}y'_{22}\right]C\right\} + A^2C\left\{2\left\|u'_1\right\|^2\left[y'_{11}y'_{12} + y'_{21}y'_{22}\right] + \left[{y'_{12}}^2 + {y'_{22}}^2 + \hbar_2\right]C\right\} + 2ABC^2\left[y'_{11}y'_{12} + y'_{21}y'_{22}\right] + B^2C\left\{2\left\|u'_2\right\|^2\left[y'_{11}y'_{12} + y'_{21}y'_{22}\right] + \left[{y'_{11}}^2 + {y'_{21}}^2 + \hbar_1\right]C\right\} + 2A^2\left\|u'_1\right\|^2 \times \left\{\left\|u'_1\right\|^2\left[{y'_{11}}^2 + {y'_{21}}^2 + \hbar_1\right]\right\} + B^2\left\|u'_2\right\|^2 \times \left\{\left\|u'_2\right\|^2\left[{y'_{12}}^2 + {y'_{22}}^2 + \hbar_2\right]\right\}\right] \tag{36}$$

$$\Delta V_C = \eta\left\{-\left(A\left\|u'_1\right\| + B\left\|u'_2\right\|\right)^2\right\} + \frac{\eta^2}{2} \times \left[\begin{matrix} \left\|u'_1\right\|^2\left({y'_{11}}^2 + {y'_{21}}^2 + \hbar_1\right) \\ \left(A^2\left\|u'_1\right\|^2 + 2ABC + B^2\left\|u'_2\right\|^2\right) \end{matrix}\right. + \left\|u'_2\right\|^2\left({y'_{22}}^2 + {y'_{12}}^2 + \hbar_2\right)\left(\begin{matrix} A^2\left\|u'_1\right\|^2 + 2ABC \\ + B^2\left\|u'_2\right\|^2 \end{matrix}\right) + 2\left(y'_{11}y'_{12} + y'_{21}y'_{22}\right) \times C\left(A^2\left\|u'_1\right\|^2 + 2ABC + B^2\left\|u'_2\right\|^2\right)\Big]$$

$$= -\eta \left(A \left\|u_1'\right\| + B \left\|u_2'\right\|\right)^2 \left[1 - \frac{\eta}{2}\left\{\left\|u_1'\right\|^2 \left[{y_{11}'}^2 + {y_{21}'}^2 + \hbar_1\right] + \left\|u_2'\right\|^2 \left[{y_{12}'}^2 + {y_{22}'}^2 + \hbar_2\right] + 2\left(y_{11}'y_{12}' + y_{21}'y_{22}'\right)C\right\}\right] \quad (37)$$

To guarantee the convergence, $\Delta V_C < 0$

$$\Rightarrow \eta \left[1 - \frac{\eta}{2}\left\{\begin{array}{l}\left\|u_1'\right\|^2 \left[{y_{11}'}^2 + {y_{21}'}^2 + \hbar_1\right] \\ + \left\|u_2'\right\|^2 \left[{y_{12}'}^2 + {y_{22}'}^2 + \hbar_2\right] \\ + 2\left(y_{11}'y_{12}' + y_{21}'y_{22}'\right)C\end{array}\right\}\right] > 0 \quad (38)$$

Consider,

$$\begin{aligned}
&\left\|u_1'\right\|^2 \left[{y_{11}'}^2 + {y_{21}'}^2 + \hbar_1\right] + \left\|u_2'\right\|^2 \times \left[{y_{12}'}^2 + {y_{22}'}^2 + \hbar_2\right] + 2\left(y_{11}'y_{12}' + y_{21}'y_{22}'\right) \times \left(\left[u_1'\right]^T \left[u_2'\right] + \left[u_2'\right]^T \left[u_1'\right]\right) \\
&= y_{11}' \left[u_1'\right]^T \left(y_{11}' \left[u_1'\right] + y_{12}' \left[u_2'\right]\right) + y_{12}' \left[u_2'\right]^T \times \begin{pmatrix} y_{22}' \left[u_1'\right] \\ + y_{22}' \left[u_2'\right] \end{pmatrix} + y_{21}' \left[u_1'\right]^T \begin{pmatrix} y_{21}' \left[u_1'\right] \\ + y_{22}' \left[u_2'\right] \end{pmatrix} \\
&\quad + y_{12}' \left[u_2'\right]^T \begin{pmatrix} y_{12}' \left[u_2'\right] \\ + y_{11}' \left[u_1'\right] \end{pmatrix} + \left[u_1'\right]^T \left[u_1'\right] \hbar_1 + \left[u_2'\right]^T \left[u_2'\right] \hbar_2 \\
&= \left\{\begin{array}{l} y_{11}' \left[u_1'\right]^T \left[y_{11}' \; y_{12}'\right] + y_{22}' \left[u_2'\right]^T \left[y_{21}' \; y_{22}'\right] \\ + y_{21}' \left[u_1'\right]^T \left[y_{21}' \; y_{22}'\right] + y_{12}' \left[u_2'\right]^T \end{array}\right. \\
&\quad \left. \times \left[y_{11}' \; y_{12}'\right] + \left[\hbar_1 \left[u_1'\right]^T \; \hbar_2 \left[u_2'\right]^T\right]\right\} \left[\begin{bmatrix} u_1' \\ u_2' \end{bmatrix}\right] \\
&= \left\{\begin{array}{l} \left[y_{11}' \; y_{12}'\right] \left[\begin{bmatrix} u_1' \end{bmatrix}^T \\ \begin{bmatrix} u_2' \end{bmatrix}^T\right] \left[y_{11}' \; y_{12}'\right] + \left[y_{21}' \; y_{22}'\right] \\ \times \left[\begin{bmatrix} u_1' \end{bmatrix}^T \\ \begin{bmatrix} u_2' \end{bmatrix}^T\right] \left[y_{21}' \; y_{22}'\right] + \left[\sqrt{\hbar_1} \; \sqrt{\hbar_2}\right] \end{array}\right. \\
&\quad \left. \times \left[\begin{bmatrix} u_1' \end{bmatrix}^T \\ \begin{bmatrix} u_2' \end{bmatrix}^T\right] \left[\sqrt{\hbar_1} \; \sqrt{\hbar_2}\right]\right\} \left[\begin{bmatrix} u_1' \\ u_2' \end{bmatrix}\right] \\
&= \left\{{y_{1c}'}^2 + {y_{2c}'}^2 + \left(\sqrt{\hbar_c}\right)^2\right\} \left[\begin{bmatrix} u_1' \end{bmatrix}^T \\ \begin{bmatrix} u_2' \end{bmatrix}^T\right] \left[\begin{bmatrix} u_1' \\ u_2' \end{bmatrix}\right] \\
&= \left\{{y_{1c}'}^2 + {y_{2c}'}^2 + \hbar_c\right\} \left[\left[u_1'\right] \left[u_2'\right]\right]^T \left[\begin{bmatrix} u_1' \\ u_2' \end{bmatrix}\right] \\
&= \left\{{y_{1c}'}^2 + {y_{2c}'}^2 + \hbar_c\right\} \left[u_c'\right]^T \left[u_c'\right] \\
&= \left\{{y_{1c}'}^2 + {y_{2c}'}^2 + \hbar_c\right\} \left\|u_c'\right\|^2
\end{aligned}$$

where, $y_{1c}' = \left[y_{11}' \; y_{12}'\right]$, $y_{2c}' = \left[y_{21}' \; y_{22}'\right]$, $\sqrt{\hbar_c} = \left[\sqrt{\hbar_1} \; \sqrt{\hbar_2}\right]$ and $\left[u_c'\right] = \left[\begin{bmatrix} u_1' \\ u_2' \end{bmatrix}\right]$

Using (38),

$$\eta \left[1 - \frac{\eta}{2}\left\{{y_{1c}'}^2 + {y_{2c}'}^2 + \hbar_c\right\} \left\|u_c'\right\|^2\right] > 0$$

$$\Rightarrow 0 < \eta < \frac{2}{\left\{{y_{1c}'}^2 + {y_{2c}'}^2 + \hbar_c\right\} \left\|u_c'\right\|^2_{\max}} \quad (39)$$

Remark 1: Since, convergence is guaranteed if the following condition is satisfied;

$$\eta \left[1 - \frac{\eta}{2}\left\{{y_{1c}'}^2 + {y_{2c}'}^2 + \hbar_c\right\} \left\|u_c'\right\|^2\right] > 0$$

Fast convergence with maximum learning rate is given as [13], [15];

$$\eta = \frac{1}{\left\{{y_{1c}'}^2 + {y_{2c}'}^2 + \hbar_c\right\} \left\|u_c'\right\|^2_{\max}} \quad (40)$$

Theorem 2: Similarly, for consequent part the ALR for parameters of each output will separately be given as;

$$0 < \eta^i < \frac{2}{\left\{\left(\frac{\partial y_1}{\partial u_i}\right)^2 + \left(\frac{\partial y_2}{\partial u_i}\right)^2 + \hbar_i\right\} \left\|\frac{\partial u_i}{\partial \boldsymbol{\theta}_i}\right\|^2_{\max}}, \quad i = 1, 2 \quad (41)$$

Proof:

For consequent part of output '1',

$\left[u_2'\right] = 0$, $\Delta e_{u_2}(k) = 0$

$$\begin{aligned}
\Delta e_1(k) &= -y_{11}' \left[u_1'\right]^T \Delta\boldsymbol{\theta} = \eta y_{11}' \left[u_1'\right]^T \frac{\partial J_C}{\partial \boldsymbol{\theta}} \\
\frac{\partial J_C}{\partial \boldsymbol{\theta}} &= \left(-e_1 y_{11}' - e_2 y_{21} + \hbar_1 u_1\right) \left[u_1'\right] \\
&\Rightarrow \Delta e_1(k) = \eta y_{11}' \left\|u_1'\right\|^2 A, \Delta e_2(k) = \eta y_{21}' \left\|u_1'\right\|^2 A, \\
\Delta e_{u_1} &= -\eta\sqrt{\hbar_1} A \left\|u_1'\right\|^2, \Delta e_{u_2} = -\eta\sqrt{\hbar_2} B \left\|u_2'\right\|^2 \quad (42) \\
&\Rightarrow \Delta V_C(k) = \eta A \left\|u_1'\right\|^2 \left(y_{11}' e_1 + y_{21}' e_2 + \sqrt{\hbar_1} e_{u_1}\right) + \frac{\Delta e_1^2}{2} + \frac{\Delta e_2^2}{2} + \frac{\Delta e_{u_1}^2}{2} < 0 \quad (43) \\
&= -\eta A^2 \left\|u_1'\right\|^2 + \frac{\eta^2}{2}\left(\left\|u_1'\right\|^2\right)^2 \left[{y_{11}'}^2 + {y_{21}'}^2 + \hbar_1\right] A^2 < 0 \\
&= -\eta A^2 \left\|u_1'\right\|^2 \left[1 - \frac{\eta}{2}\left({y_{11}'}^2 + {y_{21}'}^2 + \hbar_1\right)\left\|u_1'\right\|^2\right] < 0 \\
&\Rightarrow \eta^1 \leq \frac{2}{\left({y_{11}'}^2 + {y_{21}'}^2 + \hbar_1\right)\left\|u_1'\right\|^2} \\
&< \frac{2}{\left(\left(\frac{\partial y_1}{\partial u_1}\right)^2 + \left(\frac{\partial y_2}{\partial u_1}\right)^2 + \hbar_1\right)\left\|\frac{\partial u_1}{\partial \boldsymbol{\theta}}\right\|^2_{\max}} \quad (44)
\end{aligned}$$

Similarly, for the second output,

$$\eta^2 < \frac{2}{\left(\left(\frac{\partial y_1}{\partial u_2}\right)^2 + \left(\frac{\partial y_2}{\partial u_2}\right)^2 + \hbar_2\right)\left\|\frac{\partial u_2}{\partial \boldsymbol{\theta}}\right\|^2_{\max}} \quad (45)$$

B. STABILITY ANALYSIS OF IDENTIFIER

The identifier parameters are updated using the cost function defined as;

$$J_I = \frac{1}{2}\left(\boldsymbol{e}_I^T \boldsymbol{e}_I\right) \tag{46}$$

Here, $e_{I_i} = y_{I_i} - y_i$ is the ith entry of error vector $\boldsymbol{e_I} = \left[e_{I_1}\ e_{I_2} \cdots e_{I_k}\right]$. The generalized law for parameters adaptation is given as;

$$\hat{\boldsymbol{\theta}}_p(k+1) = \hat{\boldsymbol{\theta}}_p(k) - \hat{\boldsymbol{\eta}}\frac{\partial J_I}{\partial \hat{\boldsymbol{\theta}}_p} \tag{47}$$

where, $\hat{\boldsymbol{\theta}}_p$ and p represent the adaptation parameters vector and the corresponding output index, respectively. $\hat{\boldsymbol{\eta}}$ is the ALRs vector for identification block.

Theorem 3: Let $\hat{\eta}$be the learning rate forp th output affected by the parameter vector $\hat{\boldsymbol{\theta}}_p$ of NeuroFuzzy identifier $\hat{\boldsymbol{\Lambda}}_p$ and $\hat{\boldsymbol{\Lambda}}^p_{\mathbf{max}}$ are defined as $\hat{\boldsymbol{\Lambda}}_p = \frac{\partial y_{I_p}}{\partial \hat{\boldsymbol{\theta}}_p}$ and $\hat{\boldsymbol{\Lambda}}^p_{\mathbf{max}} = \max\left\|\hat{\boldsymbol{\Lambda}}^p\right\|$, where, $\|.\|$ is the Euclidean norm in $\Re^p$.

Then the convergence is guaranteed if the learning rates are chosen as follows;

$$0 < \hat{\eta} < \frac{2}{\left\|\frac{\partial y_{I_p}}{\partial \hat{\boldsymbol{\theta}}_p}\right\|_{\max}} \tag{48}$$

Proof:

$$V_I = \frac{1}{2}\sum_{i=1}^{2}\left(y_{d_{I_i}} - y_{I_i}\right)^2 = \frac{1}{2}\sum_{i=1}^{2} e_{I_i}^2 \tag{49}$$

$$\Delta V_I(k) = V_I(k+1) - V_I(k) \tag{50}$$

$$\Rightarrow \Delta V_I(k) = \sum_{i=1}^{2}\left(\frac{\Delta e_{I_i}^2(k)}{2} + \Delta e_{I_i}(k)\, e_{I_i}(k)\right) \tag{51}$$

Using,

$$\Delta e_{I_i} = \left[\frac{\partial e_{I_i}}{\partial \hat{\boldsymbol{\theta}}}\right]^T \Delta\hat{\boldsymbol{\theta}}, \quad \Delta\hat{\boldsymbol{\theta}} = -\hat{\boldsymbol{\eta}}\frac{\partial J_I}{\partial \hat{\boldsymbol{\theta}}}$$

$$\frac{\partial J_I}{\partial \hat{\boldsymbol{\theta}}} = \sum_{i=1}^{2} e_{I_i}\frac{\partial y_{I_i}}{\partial \hat{\boldsymbol{\theta}}}$$

$$\Rightarrow \Delta e_{I_1} = -\hat{\eta}\left\{e_{I_1}\left\|y'_{I_1}\right\|^2 + e_{I_2}\left[y'_{I_1}\right]^T\left[y'_{I_2}\right]\right\},$$

$$\Delta e_{I_2} = -\hat{\eta}\left\{e_{I_2}\left\|y'_{I_2}\right\|^2 + e_{I_1}\left[y'_{I_2}\right]^T\left[y'_{I_1}\right]\right\} \tag{52}$$

where, $y'_{I_1} = \frac{\partial y_{I_1}}{\partial \hat{\boldsymbol{\theta}}}$, $y'_{I_2} = \frac{\partial y_{I_2}}{\partial \hat{\boldsymbol{\theta}}}$

$$\begin{aligned}
&\Delta V_I(k)\\
&= -\hat{\eta}\left\{\begin{array}{l} e_{I_1}^2\left\|y'_{I_1}\right\|^2 + e_{I_1}e_{I_2}\left[y'_{I_1}\right]^T\left[y'_{I_2}\right] \\ +e_{I_1}e_{I_2}\left[y'_{I_2}\right]^T\left[y'_{I_1}\right] + e_{I_1}^2\left\|y'_{I_2}\right\|^2 \end{array}\right\}\\
&= -\hat{\eta}\left\{\left(e_{I_1}\left\|y'_{I_1}\right\| + e_{I_2}\left\|y'_{I_2}\right\|\right)^2\right\}\\
&\quad -\frac{\hat{\eta}}{2}\left\{e_{I_1}^2\left\|y'_{I_1}\right\|^4 + 2e_{I_1}e_{I_2}\left\|y'_{I_1}\right\|^2\left[y'_{I_1}\right]^T\left[y'_{I_2}\right]\right.\\
&\quad \left. +e_{I_2}^2\left\|y'_{I_1}\right\|^2\left\|y'_{I_2}\right\|^2 + e_{I_2}^2\left\|y'_{I_2}\right\|^4\right.\\
&\quad \left. +2e_{I_1}e_{I_2}\left\|y'_{I_2}\right\|^2\left[y'_{I_2}\right]^T\left[y'_{I_1}\right] + e_{I_1}^2\left\|y'_{I_1}\right\|^2\left\|y'_{I_2}\right\|^2\right.\\
&= -\hat{\eta}\left\{\left(e_{I_1}\left\|y'_{I_1}\right\| + e_{I_2}\left\|y'_{I_2}\right\|\right)^2\right.\\
&\quad -\frac{\hat{\eta}}{2}\left[\left\|y'_{I_1}\right\|^2\left(\begin{array}{l} e_{I_1}^2\left\|y'_{I_1}\right\|^2 + 2e_{I_1}e_{I_2}\left[y'_{I_1}\right]^T\left[y'_{I_2}\right] \\ +e_{I_2}^2\left\|y'_{I_2}\right\|^2 \end{array}\right)\right.\\
&\quad \left.\left. + \left\|y'_{I_2}\right\|^2\left(\begin{array}{l} e_{I_2}^2\left\|y'_{I_2}\right\|^2 + 2e_{I_1}e_{I_2}\left[y'_{I_2}\right]^T \\ \left[y'_{I_1}\right] + e_{I_1}^2\left\|y'_{I_1}\right\|^2 \end{array}\right)\right]\right\}\\
&= -\hat{\eta}\left(e_{I_1}\left\|y'_{I_1}\right\| + e_{I_2}\left\|y'_{I_2}\right\|\right)^2\left[1 - \frac{\hat{\eta}}{2}\left(\begin{array}{l}\left\|y'_{I_1}\right\|^2 \\ +\left\|y'_{I_2}\right\|^2\end{array}\right)\right]
\end{aligned} \tag{53}$$

In order to guarantee the convergence,

$$\begin{aligned}
&\left[1 - \frac{\hat{\eta}}{2}\left(\left\|y'_{I_1}\right\|^2 + \left\|y'_{I_2}\right\|^2\right)\right] > 0\\
&\Rightarrow \hat{\eta} < \frac{2}{\left\|y'_{I_1}\right\|^2 + \left\|y'_{I_2}\right\|^2} = \frac{2}{\left\|y'_{I_p}\right\|^2_{\max}}
\end{aligned} \tag{54}$$

where, $y'_{I_p} = \left[y'_{I_1}\ y'_{I_2}\right]$.

Similarly, the learning rate for parameters of consequent part corresponding to each output is given as;

$$\hat{\eta}^p < \frac{2}{\left\|y'_{I_p}\right\|^2_{\max}} \tag{55}$$

V. SIMULATION RESULTS: TEMPORAL, SPECTRAL AND NUMERICAL

Fig. 3 shows two area, four machines benchmark test system for the performance validation of suggested control paradigms. MATLAB/SIMULINK software has been used for system and control implementation. The complete details of system parameters and load flow settings can be found in [12]. PSSs installed in the whole system are disabled to elude the chances of destabilizing interaction and the whole damping is provided using FACTS only. The simulations have been carried out for open-loop environment, with no damping control installed in the system and for closed-loop system equipped with ANFTSC and HBsWC based FACTS. In ANFTSC scheme both the identification and control block are simple NeuroFuzzy TSK structure, whereas, in case of HBsWC the control block utilizes the HBsW architecture

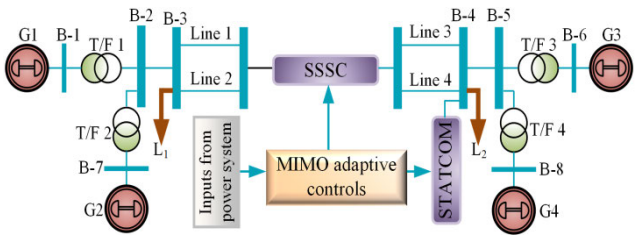

FIGURE 3. Benchmark test system.

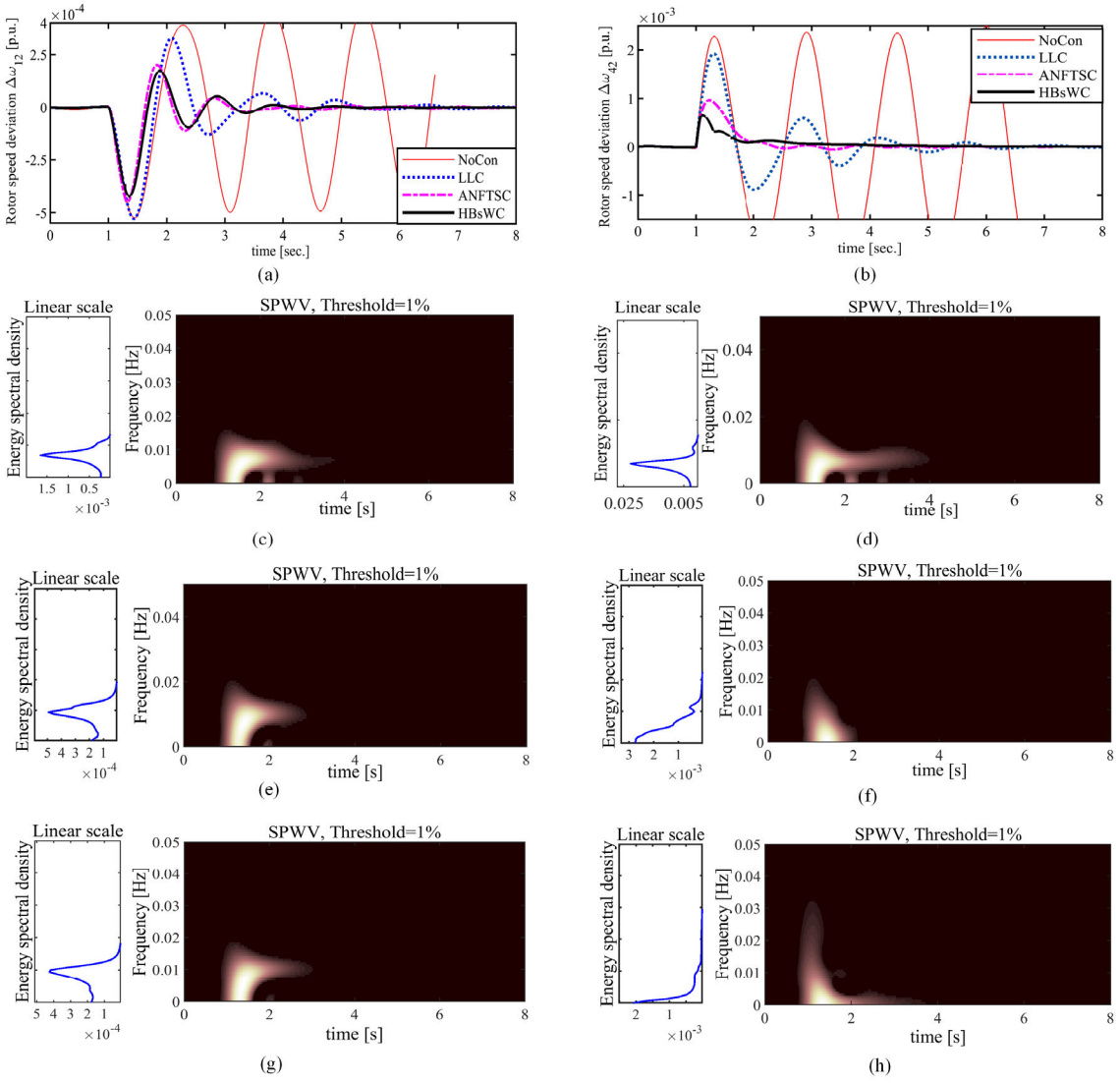

FIGURE 4. Scenario-I (a) Local modes, (b) Inter-area modes, (c) LLC local mode spectrum, (d) LLC inter-area mode spectrum, (e) ANFTSC local mode spectrum, (f) ANFTSC inter-area mode spectrum, (g) HBsWC local mode spectrum, (h) HBsWC inter-area mode spectrum.

shown previously in Fig. 2 and identification block utilizes NeuroFuzzy TSK structure.

Furthermore, the comparative study has also been made using frequency domain analysis based on Smoothed-Pseudo Wigner Ville Distribution (SPWVD) and different performance indices. The performance indices and frequency domain analysis give insight regarding the performance of a control algorithm in transient and steady-state region and energy content for different frequencies, respectively.

The general formula for performance index is given as;

$$PI = \int_0^{t_s} t^u \left| \sum_{i=1}^{n} (\Delta\omega_{L_i} + \Delta\omega_{I_i}) \right|^v dt \tag{56}$$

where, 'n' shows total number of modes.

LIMOs are denoted by L and I with t_s being the complete simulation time. Also, u and v are constants, such that $(u, v) = (0, 1)$ corresponds to Integral Absolute Error (IAE), $(u, v) = (0, 2)$ corresponds to Integral Time Absolute Error (ITAE), $(u, v) = (1, 1)$ corresponds to Integral Square Error (ISE) and $(u, v) = (1, 2)$ corresponds to Integral Time Square Error (ITSE).

SPWVD is calculated as;

$$SPWVD_x(k, \omega) = \int_{-\infty}^{\infty} h(\tau) \int_{*(u-\tau/2)du e^{-j\omega\tau}}^{g(u-k)x(u+\tau/2)x} d\tau \tag{57}$$

Here, $g(k)$ and $h(\tau)$ is the time domain smoothing function and frequency smoothing window, respectively. $h(\tau)$ reduces the cross-terms effect and removes the integration over $]-\infty\infty[$ for WVD [14].

In what follows is the detail of different fault scenarios:

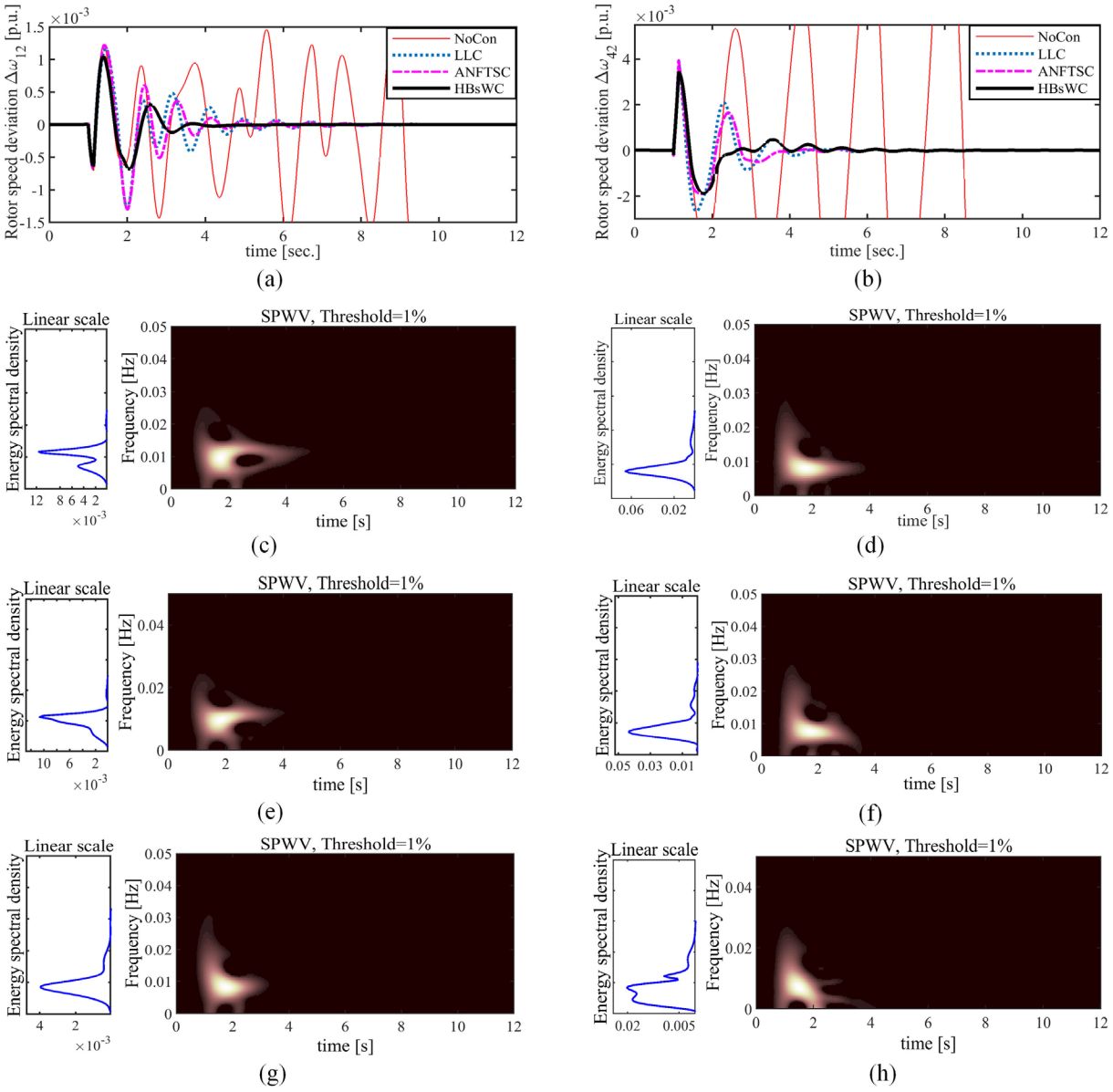

FIGURE 5. Scenario-II (a) Local modes, (b) Inter-area modes, (c) LLC local mode spectrum, (d) LLC inter-area mode spectrum, (e) ANFTSC local mode spectrum, (f) ANFTSC inter-area mode spectrum, (g) HBsWC local mode spectrum, (h) HBsWC inter-area mode spectrum.

A. SCENARIO-I

The performance against small disturbance was checked using load reduction in L_2, at $t = 1$ sec.

Fig. 4 shows the simulation results for this fault scenario. Figures 4(a) and 4(b) show the simulation results for LIMOs. The results reveal that in case of no damping control the system loses its synchronism when subjected to this fault. The application of conventional LLC makes the system to regain its equilibrium with poorly damped oscillations. ANFTSC and HBsWC efficiently restore the system, however, their damping improvement is comparable for this small fault, especially, for LMOs.

Figures 4 (b)-(h) show the frequency domain results of LLC, ANFTSC and HBsWC along with the energy content of frequency spectra. The results reveal that all control paradigms have almost same energy content of frequency spectra for LMOs, however, in case of IMOs HBsWC has lowest energy for low frequencies.

B. SCENARIO-II

A 3-φ fault for duration of 8-cycles with self-clearing feature has been applied on line 4 to analyze the controller performance against large disturbance, at $t = 1$ sec. Fig. 5 shows the performance results for this scenario. The results for LIMOs are shown in Figs. 5(a) and 5(b). The results reveal that system loses its synchronism when no damping control is installed in the system.

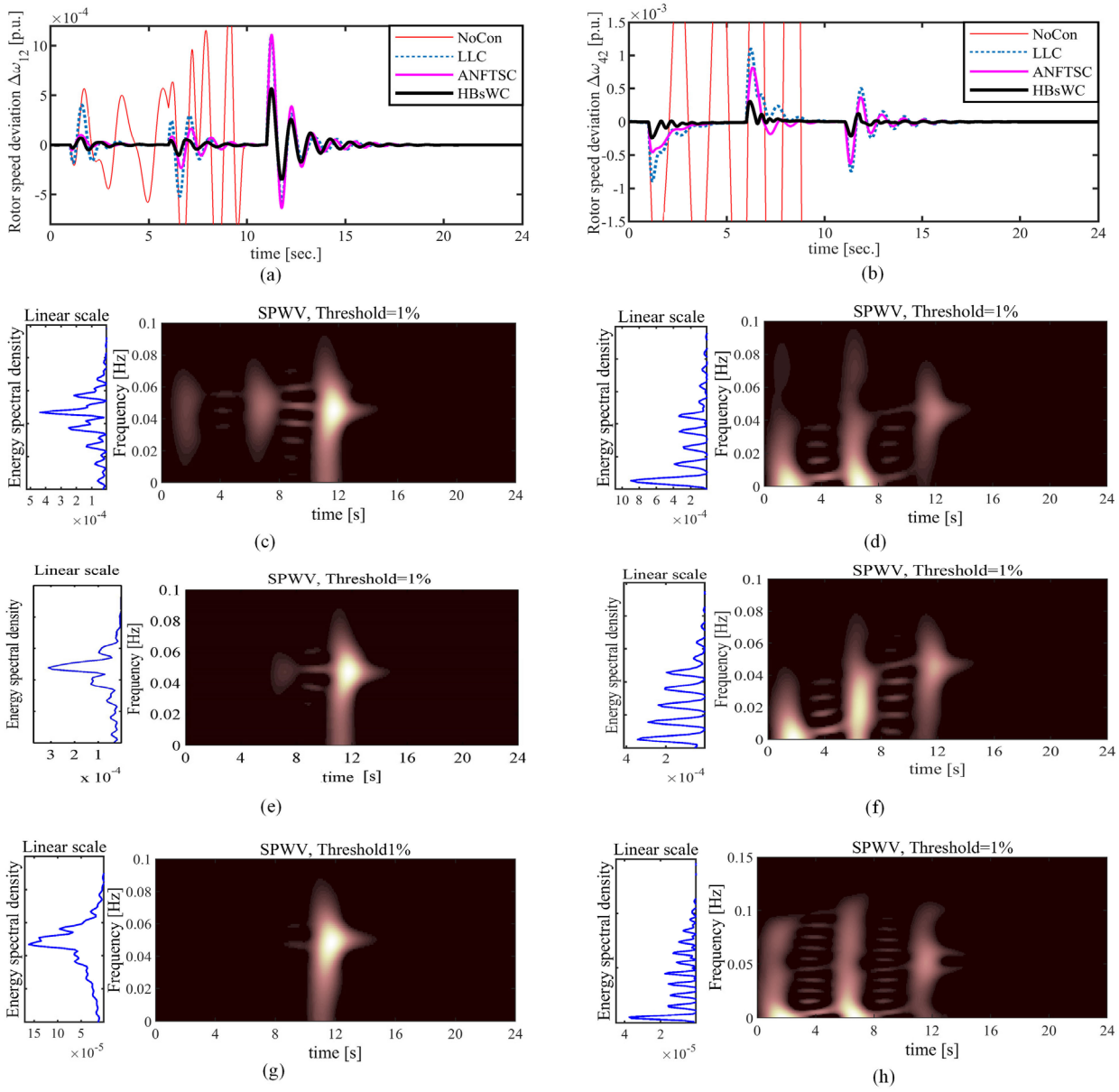

FIGURE 6. Scenario-III (a) Local modes, (b) Inter-area modes, (c) LLC local mode spectrum, (d) LLC inter-area mode spectrum, (e) ANFTSC local mode spectrum, (f) ANFTSC inter-area mode spectrum, (g) HBsWC local mode spectrum, (h) HBsWC inter-area mode spectrum.

The damping performance of LLC and ANFTSC is almost the same, however, HBsWC gives significant performance improvement. The frequency domain results given in Figs. 5(c)-5(h) reveal that in case of LLC and ANFTSC the low frequencies have very high energy content for LIMOs, whereas, the energy content of low frequency spectra is small for HBsWC.

C. SCENARIO-III

In order to validate the online stability and robustness of the proposed control strategies, multiple faults have been applied to the system. Initially, line 2 has been temporarily removed from the system at t = 1 sec. for a duration of 5 secs. and then reconnected at t = 6 secs. to restore the system. Another fault of 10% step increase in mechanical input of generator G1 in area 1, has been applied as third fault event, at t = 11 secs.

Fig. 6 presents the simulation results for this scenario. The time domain results presented in Figs. 6(a) and 6(b) show that in case of no control the system becomes unstable before the occurrence of third fault.

LLC and ANFTSC give poorly damped oscillatory behavior, whereas, HBsWC effectively restores the system equilibrium to maintain the performance at different operating conditions. The frequency domain results, for LMOs, presented in Figs. 6(c), 6(e) and 6(f) show that the energy

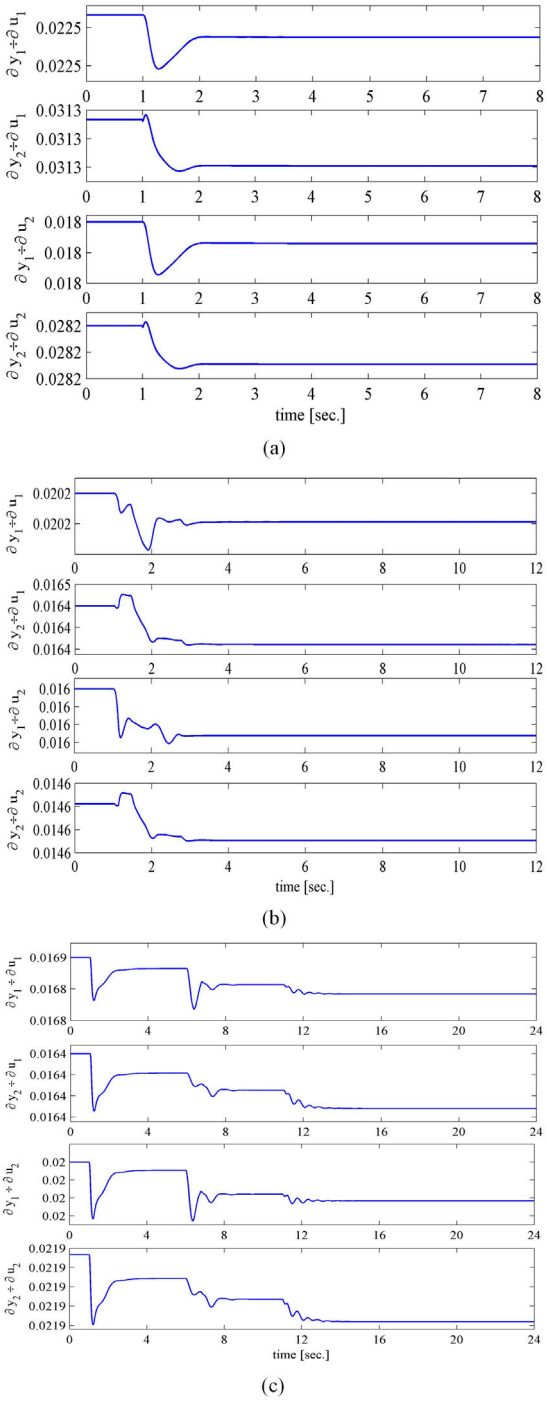

FIGURE 7. Plant Jacobean for ANFTSC (a) Scenario-I, (b) Scenario-II, (c) Scenario-III.

content for all the three faults is significant in case of LLC. ANFTSC suppresses the energy content for first fault but it fails to fully eliminate the energy content of last two faults.

On the other hand, HBsWC has almost zero energy content for first two faults and very small energy content of short duration for third fault. The results for IMOs, shown in Figs. 6(d), 6(f) and 6(h), reveal that energy content for proposed HBsWC has lowest magnitude for all the three faults as depicted clearly in the given linear scale ESD.

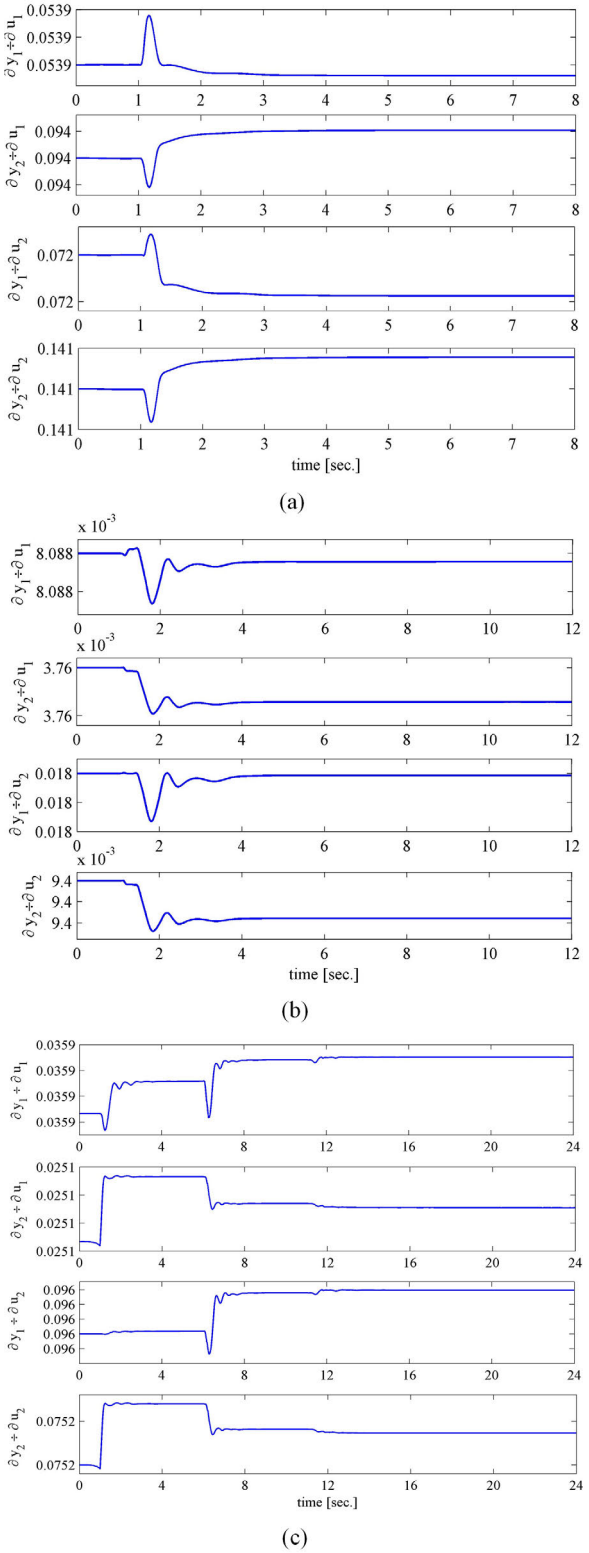

FIGURE 8. Plant Jacobean for HBsWC (a) Scenario-I, (b) Scenario-II, (c) Scenario-III.

The plant model is estimated online using Jacobean for which the results are shown in Figs. 7 and 8, for all the three scenarios.

TABLE 1. Time and frequency domain performance improvement w.r.t. Lead-Lag Control [%].

Test Scenarios	Control Algorithm	Time Domain Performance Index				Frequency Domain ESD	
		ITAE	ITSE	IAE	ISE	LMOs	IMOs
Scenario-I	ANFTSC	68.73	83.98	62.15	80.56	51.77	78.38
	HBsWC	73.52	93.12	71.43	92.26	54.88	92.39
Scenario-II	ANFTSC	14.85	27.60	13.21	24.29	-4.76	20.16
	HBsWC	52.37	68.60	47.66	62.01	49.21	35.35
Scenario-III	ANFTSC	19.47	35.24	27.50	45.59	16.34	44.80
	HBsWC	57.62	76.46	64.66	82.77	41.81	94.39

The statistical results for performance improvement are presented in Table 1. The results show that ANFTSC shows competitive results w.r.t. LLC for small faults and the performance margin between ANFTSC and HBsWC is small.

However, for large faults and more complex scenarios like series of faults the performance difference is significant highlighting the superior performance of proposed HBsWC. Furthermore, large values of ITSE and ISE as compared to ITAE and IAE show more pronounced effect of proposed control strategy in transient region as compared to that in steady-state region.

Table 1 also summarizes the frequency domain analysis quantified on the basis of ESD. The results show the percentage improvement in terms of the energy content of low frequencies. The statistics reveal that HBsWC has significantly improved performance as compared to LLC and ANFTSC for both LIMOs in all the three scenarios. However, it has been observed that performance improvement for ANFTSC is small in case of large fault as considered in scenario-II. ANFTSC suffers performance degradation as compared to LLC for LMOs in scenario-II.

It is due to the fact that although the maximum value of ESD is high for LLC as compared to that of ANFTSC, as shown in Fig. 5(e), but the spectrum of ANFTSC has more values of higher magnitude as compared to LLC.

This also signifies the importance of quantitative results for ESD by revealing the aspects not observable in graphical results, shown in Figs. 4-6. However, the proposed HBsWC maintains its superior performance in all scenarios.

VI. CONCLUSION

This article presents MIMO online indirect adaptive NeuroFuzzy control techniques and the comparative evaluation of different variants of conventional and advanced antecedent and consequent parts based on nonlinear time and frequency domain analysis. The proposed control scheme suffers no offline training overhead and updates the parameters using current value of the plant Jacobean.

The performance of the proposed control schemes is validated based on comparison with conventional Lead-Lag control using different fault scenarios and evaluation criterion. It has been found that the proposed HBsWC gives supreme performance improvement for both LIMOs in a power system installed with multi-type FACTS. The results reveal that although the generic TSK structure with ALRs may give competitive performance improvement for small faults. However, for large faults, there is significantly large performance improvement margin between HBsWC and ANFTSC.

Furthermore, the quantitative analysis of frequency domain results reveals that conventional NeuroFuzzy controls may suffer performance degradation for large faults. However, the proposed HBsWC is robust and retains its performance excellence for all cases as revealed by temporal, spectral and numerical analysis.

The control scheme investigated in this work has many interesting future research directions to be investigated for further performance improvement. Mainly the control performance can be investigated for optimization by using some advanced optimization technique like Levenberg-Marquardt and recurrent network structure. Use of sliding mode control by introducing a sliding surface in consequent part can also be investigated for control effort smoothness. Also, the advancement in hardware in-loop simulation tools have opened a new research dimension for investigation of these complex control techniques from theory to practice.

REFERENCES

[1] E. Larsen, J. Sanchez-Gasca, and J. Chow, "Concepts for design of FACTS controllers to damp power swings," *IEEE Trans. Power Syst.*, vol. 10, no. 2, pp. 948–956, May 1995.

[2] C.-F. Lu, C.-H. Hsu, and C.-F. Juang, "Coordinated control of flexible AC transmission system devices using an evolutionary fuzzy lead-lag controller with advanced continuous ant colony optimization," *IEEE Trans. Power Syst.*, vol. 28, no. 1, pp. 385–392, Feb. 2013.

[3] A. Kazemi and M. V. Sohrforouzani, "Power system damping using fuzzy controlled facts devices," *Int. J. Electr. Power Energy Syst.*, vol. 28, no. 5, pp. 349–357, Jun. 2006.

[4] J.-W. Park, R. Harley, and G. Venayagamoorthy, "New external neuro-controller for series capacitive reactance compensator in a power network," *IEEE Trans. Power Syst.*, vol. 19, no. 3, pp. 1462–1472, Aug. 2004.

[5] M. Alizadeh and M. Tofighi, "Full-adaptive THEN-part equipped fuzzy wavelet neural controller design of FACTS devices to suppress inter-area oscillations," *Neurocomputing*, vol. 118, pp. 157–170, Oct. 2013.

[6] M. O. Sadegh and K. L. Lo, "Decentralized coordination of FACTS devices for power system stability enhancement using intelligent programming," *Int. J. Comput. Math. Electr. Electron. Eng.*, vol. 24, pp. 179–201, Mar. 2005.

[7] R. Badar and L. Khan, "Power system oscillations damping using HABsW based FACTS-SSSC," *J. Intell. Fuzzy Syst.*, vol. 27, no. 3, pp. 1575–1587, 2014.
[8] P. Jiang, Z. Fan, S. Feng, X. Wu, H. Cai, and Z. Xie, "Mitigation of power system forced oscillations based on unified power flow controller," *J. Mod. Power Syst. Clean Energy*, vol. 7, no. 1, pp. 99–112, Jan. 2019.
[9] S. Xu, L. Gao, H. Sun, B. Zhao, P. Wu, C. Lv, and J. Bi, "Coordinated damping control for power system dynamic stability based on wide-area expert system," in *Proc. Chin. Control Decis. Conf. (CCDC)*, Nanchang, China, 2019, pp. 4094–4099.
[10] N. A. Arzeha, M. W. Mustafa, and R. M. Idris, "Damping low frequency oscillations via FACTS-POD controllers tuned by bees algorithm," *J. Electr. Eng.*, vol. 17, no. 2, pp. 6–14, 2018.
[11] L. H. Hassan, M. Moghavemmi, H. A. F. Alburib, K. M. Muttaqi, and H. Du, "Damping of low-frequency oscillations and improving power system stability via auto-tuned PI stabilizer using Takagi-Sugeno fuzzy logic," *Int. J. Electr. Power Energy Syst.*, vol. 38, no. 1, pp. 72–83, 2012.
[12] R. Badar and L. Khan, "Legendre wavelet embedded NeuroFuzzy algorithms for multiple FACTS," *Int. J. Electr. Power Energy Syst.*, vol. 80, pp. 81–90, Sep. 2016.
[13] R. Badar, "Adaptive soft computing synergistic paradigms for VSC based FACTS damping controls," Ph.D. dissertation, Dept. Elect. Eng., COMSATS University Islamabad, Islamabad, Pakistan, 2014.
[14] S. Case, "Time-frequency analysis of systems with changing dynamic properties," Ph.D. dissertation, California Inst. Technol., Pasadena, CA, USA, 2006.
[15] R. Badar and L. Khan, "Coordinated adaptive control of multiple flexible AC transmission systems using multiple-input—Multiple-output neuro-fuzzy damping control paradigms," *Electr. Power Compon. Syst.*, vol. 42, no. 8, pp. 818–830, 2014.

RABIAH BADAR received the M.S. degree in computer engineering and the Ph.D. degree in electrical engineering from COMSATS University Islamabad, Islamabad, in 2007 and 2009, respectively. From February 2015 to May 2015, she was an Assistant Professor with the Namal College, Mianwali, Pakistan. Since June 2015, she has been an Assistant Professor with COMSATS University Islamabad. She is the author of many international, peer-reviewed journal research articles, conference papers, and book chapters. She has successfully supervised many undergraduate and graduate research thesis. Her research interests include artificial intelligence, optimization, soft computing, power system stability and control, nonlinear adaptive control, FACTS, HVDC, and renewable energy systems.

MOHAMMAD ZUBAIR KHAN received the Master of Technology degree in computer science and engineering from U.P. Technical University, Lucknow, India, in 2006, and the Ph.D. degree in computer science and information technology from the Faculty of Engineering, M.J.P. Rohilkhand University, Bareilly, India. Past he has worked as the Head and an Associate professor with the Department of Computer Science and Engineering, Invertis University, Bareilly. He is currently an Associate Professor with the Department of Computer Science, College of Computer Science and Engineering, Taibah University. He has published more than 40 journals and conference papers. His current research interests are data mining, big data, parallel and distributed computing, theory of computations, and computer networks. He has more than 15 years teaching and research experience. He has been a member of Computer Society of India, since 2004.

MUHAMMAD AWAIS JAVED (Senior Member, IEEE) received the B.Sc. degree in electrical engineering from the University of Engineering and Technology, Lahore, Pakistan, in August 2008, and the Ph.D. degree in electrical engineering from The University of Newcastle, Australia, in February 2015. From July 2015 to June 2016, he was a Postdoctoral Research Scientist with the Qatar Mobility Innovations Center (QMIC) on SafeITS project. He is currently an Assistant Professor with COMSATS University Islamabad, Pakistan. His research interests include intelligent transport systems, vehicular networks, protocol design for emerging wireless technologies, and the Internet of Things.